White Holes in the Fresnel Zone Causing Ambiguous First Arrival Time Tomography Interpretation

Shimon Coen
Geofronts Inc., P.O. Box 7038, Berkeley, California 94707
and CCS, Lawrence Berkeley Laboratory, Berkeley, California 94720
(Received 30 December 1993)

It is shown that complete and precise first arrival time tomography data are not capable of uniquely reconstructing certain realistic velocity distributions. The nonuniqueness is demonstrated by different velocity distributions that share identical first arrival time data. In these examples, the combined Fresnel zone for all source and receiver combinations do not cover the entire imaging region and leave there uncovered regions we call white holes.

PACS numbers: 43.35.+d, 42.30.Wb, 87.59.Fm

The goal of first arrival time tomography is to infer the velocity distribution within a bounded region from first arrival time measurements performed at the boundary of the region. This method of probing an inaccessible medium is used in medical imaging, geophysical imaging, and the nondestructive testing of materials and processes. These applications demand and deserve tomography results that correspond to reality, i.e., adequately approximate the true velocity distribution within the probed region. Any ambiguities resulting from this imaging method must be analyzed and reported in order to avoid erroneous interpretation. In this Letter we demonstrate that the reconstruction of the velocity distribution from complete and precise first arrival time tomography data is generally not unique. This nonuniqueness can lead to ambiguous first arrival time tomography interpretation. Nonuniqueness caused by different parametrization of the unknown velocity distribution and by incomplete and imprecise first arrival time tomography data will not be treated here. This allows the separation of the nonuniqueness of the inverse problem into component parts by studying first the intrinsic features of the inverse problem with complete and precise data and then dealing separately with how the other sources of nonuniqueness make the task of inferring the velocity distribution even more difficult.

Our study of the nonuniqueness of the inverse problem of first arrival time tomography with complete and precise data is performed without using any inversion algorithm. This allows us to draw conclusions about the inverse problem without any interference from the particular inversion algorithm used in the reconstruction of the velocity distribution. We note, however, that an inversion algorithm may introduce additional sources of nonuniqueness, i.e., by producing a velocity distribution corresponding to a local rather than a global minimum in the misfit measure between the measured data and the data corresponding to the reconstructed velocity distribution.

The practical inverse problem of first arrival time tomography is often formulated as a nonlinear optimization problem. The results from our nonuniqueness study can be used to explore the existence of distinct global minima in the associated nonlinear optimization problems. As will be shown in this Letter, such distinct global minima exist with zero minima, i.e., different velocity distributions that share identical first arrival time tomography data.

In the short wavelength limit, the first arrival time is modeled by the value of the line integral of the slowness (reciprocal velocity) along the first arrival ray joining the source and receiver. Complete first arrival time tomography data [1] consist of the first arrival time for all possible source and receiver combinations at the boundary of the probed region. It is usually assumed that complete and precise first arrival time tomography data uniquely determine the velocity distribution. This assumption is based on the premise that complete first arrival time tomography data are produced by rays that cover the entire probed region. When diffraction [2] contributes to the first arrival rays, certain regions we call white holes are not covered by any first arrival rays. Under certain conditions, the complete first arrival time tomography data are independent of the velocity distribution in the white holes, and this leads to nonuniqueness and erroneous interpretations.

This fundamental ambiguity is quantified next by using two specific examples in 2D, as shown in Fig. 1 (top panels), where both examples contain a uniform slow velocity anomaly relative to a uniform background velocity. The first arrival ray, joining the source S and receiver R, will be the diffracted ray [3] that touches the exterior side of the boundary of the anomaly, and not the refracted ray through the anomaly, provided that

$$c_0/c_i > 0.5\Big[\sqrt{\xi^2 - 1} + \sqrt{\eta^2 - 1} + \arcsin(1/\xi) + \arcsin(1/\eta) + 2 - \xi - \eta\Big] \quad (1)$$

is satisfied for the circular anomaly, provided that

$$c_o/c_i > 0.5\Big(\sqrt{\beta^2 + 1} + \sqrt{\mu^2 + 1} + 2 - \beta - \mu\Big) \quad (2)$$

0031-9007/94/73(24)/3219(4)$06.00

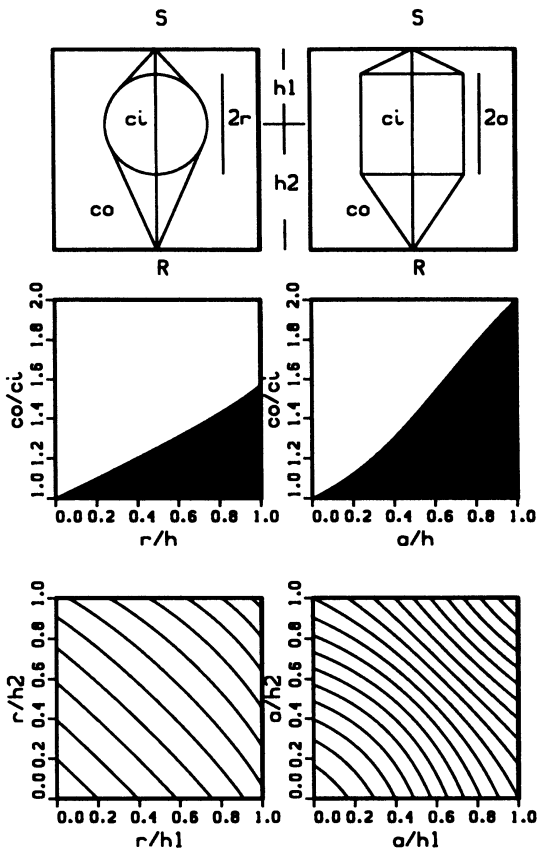

FIG. 1. Top panels show the geometry for the circle and square anomalies. Middle panels represent $h_1 = h = h_2$, where the white zone corresponds to diffracted first arrivals and the black zone corresponds to refracted first arrivals. Bottom panels represent $h_1 \neq h_2$, where the contours start with $c_o/c_i = 1.05$ at the bottom left of each panel and increase upward by increments of 0.05.

is satisfied for the square anomaly, where $\xi = h_1/r$, $\eta = h_2/r$, $\beta = h_1/a - 1$, $\mu = h_2/a - 1$. These equations were derived from the travel time for the diffracted and refracted rays. The conditions (1) and (2) are displayed in Fig. 1 for $h_1 = h_2$ (middle panels) and for $h_1 \neq h_2$ (bottom panels) for the circle (left) and for the square (right). When complete and precise first arrival time tomography data is available on the boundary of a circle of radius h centered at either the circle or the square anomaly, then the white zone in the middle panels is a nonuniqueness zone where white holes live. The black zone in these panels is a uniqueness zone where white holes do not exist. Lowering the velocity distribution in the white holes will not change the first arrival time tomography data. Unique reconstruction of the velocity distribution in the white holes is thus impossible, and, consequently, the interpretation will be erroneous.

When $c_o/c_i > \pi/2$ for the circular anomaly and $c_o/c_i > 2$ for the square anomaly, the nonuniqueness exists, and it is independent of a and r and the position of either anomaly. When either anomaly is symmetrical with respect to the boundary of a circular probed region of radius h and $r \ll h$ for the circle [4] and $a \ll h$ for the square, then nonuniqueness can exist for extremely low contrast in velocity, provided that $c_o/c_i > 1 + r/2h$ for the circle and $c_0/c_i > 1 + a/2h$ for the square.

So far we have dealt with the fundamental ambiguity of first arrival time tomography in 2D by using rays of zero thickness. Under certain conditions these mathematical rays produce a white hole in the imaging region. Here we demonstrate the effect of frequency, within the short wavelength limit, on the white hole, by constructing the Fresnel zone [2] associated with the first arrival rays for the square anomaly (top right panel in Fig. 1). Any position X within the Fresnel zone of the first arrival ray associated with the source position X_s and the receiver position X_r satisfies the inequality

$$T(X_s, X) + T(X_r, X) - T(X_s, X_r) \leq 0.5/f\,, \qquad (3)$$

where $T(A, B)$ is the first arrival time at B due to a source at A, and f is the frequency. Figure 2 shows the Fresnel zone for the square anomaly for six combinations of sources and receivers at the boundary of the probed region which is also a square but larger than the square anomaly. Figure 2 contains two groups where the size of the square anomaly decreases from group 2(a) to group 2(b). There are six panels in each group where the top three panels represent frequency $4f$ and the bottom panels represent

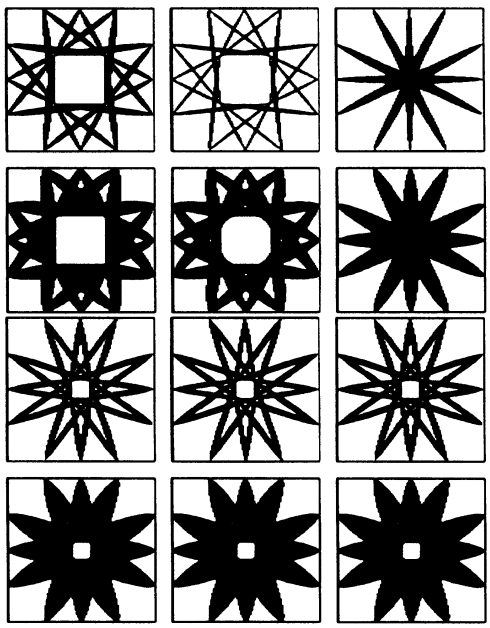

FIG. 2. (a) Combined Fresnel zones for decreasing contrast (left to right) and decreasing frequency from $4f$ (top) to f (bottom). Here c_i/c_o has the value 0.5 (left), 0.75 (middle), and 0.85 (right). The size of the square anomaly is $\frac{1}{3}$ of the size of the concentric boundary, i.e., $a/h = \frac{1}{3}$. (b) Combined Fresnel zones as in (a) but for a smaller size square anomaly, i.e., $a/h = \frac{1}{9}$.

frequency f. In each group the contrast decreases from left to right. The main conclusions to be drawn from these combined Fresnel zones are (i) reducing the frequency generally reduces slightly the size of the white hole, and (ii) the lowest contrast anomaly contains a white hole when its size is small [right panels of Fig. 2(b)] and is free of a white hole when its size is large [right panels of Fig. 2(a)]. The first arrival time map needed for these Fresnel zones was computed by a new numerical implementation of Huygens' construction [5] which will be reported elsewhere.

We have demonstrated that certain realistic and simple velocity distributions of varying contrast and size cannot be uniquely reconstructed from complete and precise first arrival time tomography data in the short wavelength limit. These velocity distributions share identical first arrival time tomography data, and therefore the associated nonlinear optimization problem has distinct global minima. Each such minima corresponds to a different velocity distribution, and, consequently, it is impossible to reconstruct the true velocity distribution from these data. This is a major deficiency of the first arrival time tomography data in the special cases that we have dealt with in this Letter, as well as in other cases where the velocity distribution allows for the existence of a white hole. We suspect that such white holes exist unnoticed in various published and unpublished results and even in recent lecture notes, an example of which is discussed next.

In an innovative application of Fermat's principle, Berryman [6] adjusts the step size of the nonlinear damped least squares, at each iteration, so as to essentially minimize the number of reconstructed rays that arrive earlier than the corresponding measured first arrival time. He shows reconstruction obtained by the algorithm in three different synthetic examples corresponding to 20%, 50%, and 100% contrast in slowness (each containing a low and high slowness anomaly relative to a uniform background), and based on these, he claims that the algorithm "produces very good reconstruction even for high contrast material where standard methods tend to diverge." We demonstrate, however, that the velocity distributions corresponding to 50% and 100% contrast cannot be uniquely reconstructed by any inversion algorithm, because they contain a white hole larger than the cell size used in the model parametrization. We computed the first arrival time map and the Fresnel zone for Berryman's examples by discarding the high velocity anomaly and focusing only on the low velocity anomaly and its vicinity in order to temporarily eliminate any interference from the high velocity anomaly. The geometrical wave fronts for a single source position and for the three different contrasts are shown in Fig. 3. The resulting Fresnel zone for 50 source/receiver combinations are shown in Fig. 4 for the three contrasts and for two different frequencies, f (bottom panels) and $4f$ (top panels). These combined Fresnel zones show a large white hole in the 100% and 50% contrast for both frequencies, small white holes for the 20% contrast and frequency $4f$ and no white holes for the corresponding frequency f (small and large are relative to the

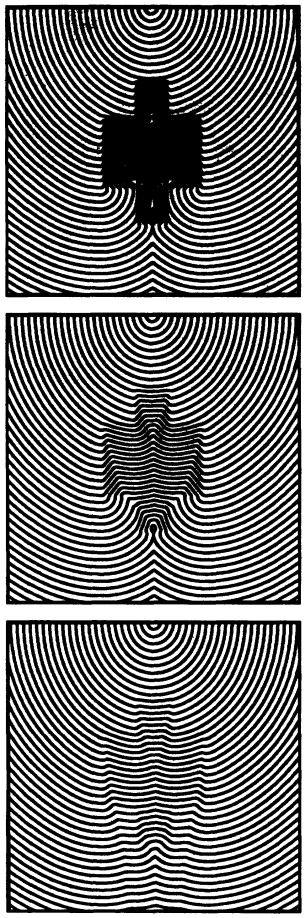

FIG. 3. Geometrical wave fronts for a fixed source position and decreasing contrast from top to bottom, i.e., $c_o/c_i = 2.0$ (top), $c_o/c_i = 1.5$ (middle), and $c_o/c_i = 1.2$ (bottom).

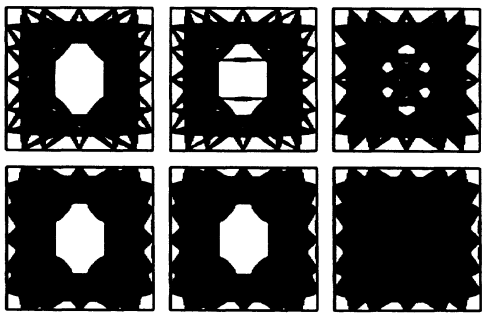

FIG. 4. Combined Fresnel zones for contrast in slowness of 100% (left), 50% (middle), 20% (right), and frequency $4f$ (top) and f (bottom) for Berryman's low velocity anomaly using 50 source/receiver combinations.

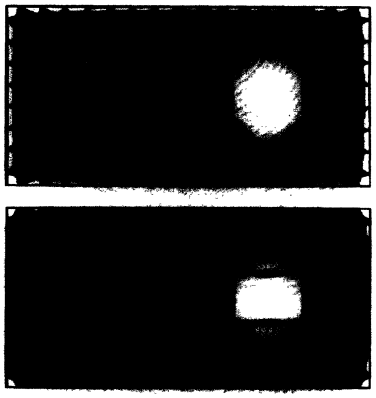

FIG. 5. White holes in Berryman's 50% contrast model for frequency $4f$ (top) and f (bottom) for all the 320 source/receiver combinations.

cell size used in the model parametrization). Therefore, the low velocity anomaly in Berryman's 50% and 100% contrast models cannot be uniquely reconstructed by an inversion algorithm. These results also demonstrate why the inversion results for the 50% and 100% contrasts were not as good as the inversion results for the 20% contrast. We also computed the Fresnel zone for the 320 source/receiver combinations used by Berryman in his 50% contrast model, the results of which are shown in Fig. 5 for frequency f (bottom panel) and frequency $4f$ (top panel). Both panels show a large white hole at the low velocity anomaly. Therefore, this example (and the 100% contrast not shown) possess distinct global minima, corresponding to different velocity distributions (lowering the velocity in the white hole) that cannot be unambiguously determined by Berryman's algorithm or any other inversion algorithm. It is interesting to note that Berryman uses a fast ray tracer that allows for Fermat's principle to be violated, the same principle that his inversion algorithm is based upon. There is, however, a double violation of this principle in the generation of the synthetic data and in the iterative solution of the nonlinear inverse problem.

The major conclusion of this Letter is that complete and precise first arrival time tomography data cannot uniquely reconstruct the velocity distribution in the presence of white holes. Lowering the velocity in these white holes does not alter the first arrival time tomography data and this leads to erroneous velocity interpretation.

It is a pleasure to acknowledge useful discussions with Keith Miller.

[1] S. A. Johnson *et al.*, in *Proceedings of the Ultrasonic Symposium, Boston, 1975* (IEEE, New York, 1975) pp. 44–51.
[2] A. Fresnel, Ann. Chim. Phys. **2**, 239 (1816).
[3] J. B. Keller, J. Appl. Phys. **28**, 426 (1957).
[4] C. G. McKinnon and R. H. T. Bates, Ultrasonic Imaging **2**, 48 (1980).
[5] C. Huygens, *Traité de la lumière,* (Van der Aa, Leiden, 1690).
[6] J. G. Berryman, Phys. Rev. Lett. **62**, 2953 (1989); Inverse Problems **6**, 21 (1990); Int. J. of Imaging Systems and Tech. **2**, 112 (1991); Lecture Notes on Nonlinear Inversion and Tomography, LLNL Report No. UCRL-LR-105358-Rev. 1991.

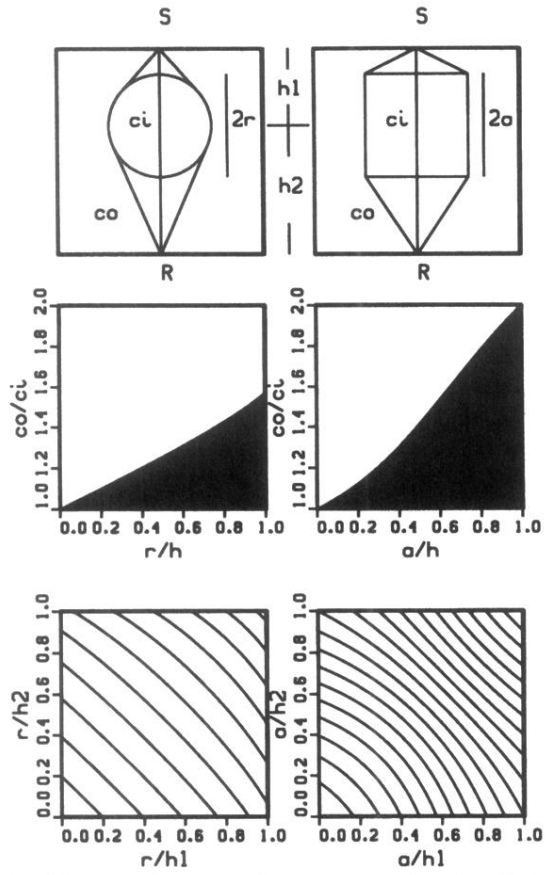

FIG. 1. Top panels show the geometry for the circle and square anomalies. Middle panels represent $h_1 = h = h_2$, where the white zone corresponds to diffracted first arrivals and the black zone corresponds to refracted first arrivals. Bottom panels represent $h_1 \neq h_2$, where the contours start with $c_o/c_i = 1.05$ at the bottom left of each panel and increase upward by increments of 0.05.

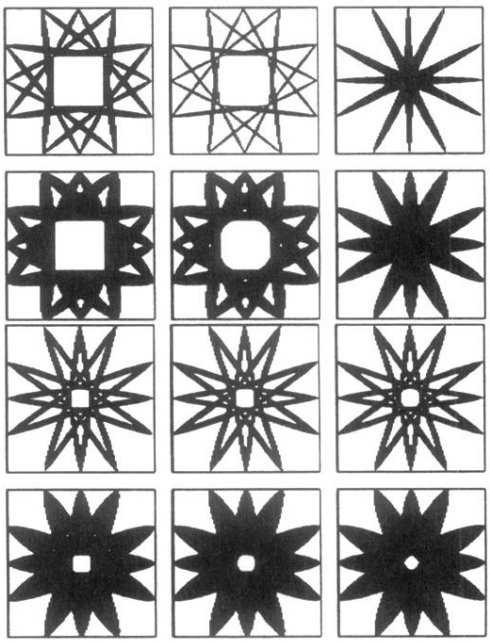

FIG. 2. (a) Combined Fresnel zones for decreasing contrast (left to right) and decreasing frequency from $4f$ (top) to f (bottom). Here c_i/c_o has the value 0.5 (left), 0.75 (middle), and 0.85 (right). The size of the square anomaly is $\frac{1}{3}$ of the size of the concentric boundary, i.e., $a/h = \frac{1}{3}$. (b) Combined Fresnel zones as in (a) but for a smaller size square anomaly, i.e., $a/h = \frac{1}{9}$.

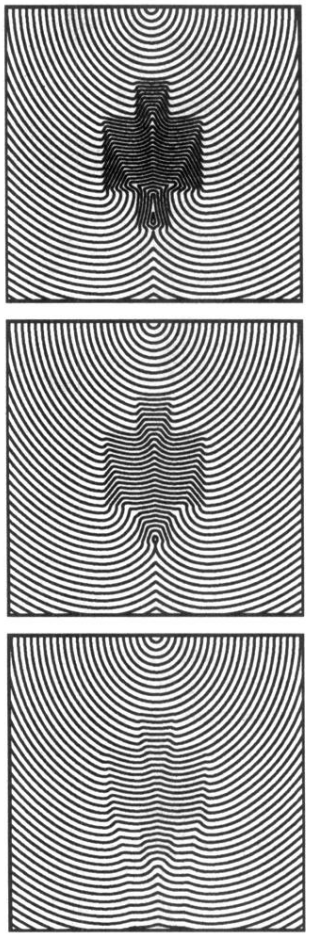

FIG. 3. Geometrical wave fronts for a fixed source position and decreasing contrast from top to bottom, i.e., $c_o/c_i = 2.0$ (top), $c_o/c_i = 1.5$ (middle), and $c_o/c_i = 1.2$ (bottom).

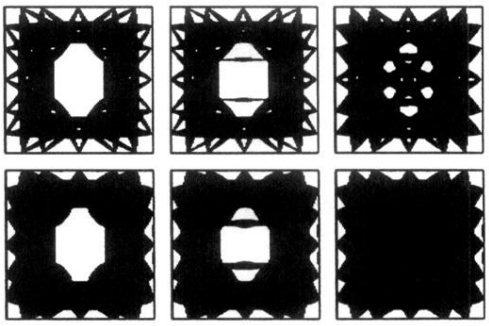

FIG. 4. Combined Fresnel zones for contrast in slowness of 100% (left), 50% (middle), 20% (right), and frequency $4f$ (top) and f (bottom) for Berryman's low velocity anomaly using 50 source/receiver combinations.

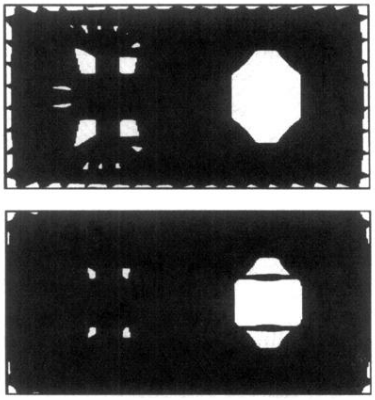

FIG. 5. White holes in Berryman's 50% contrast model for frequency $4f$ (top) and f (bottom) for all the 320 source/receiver combinations.